



## OPEN ACCESS

## EDITED BY

Francisca Martinez-Ruiz,  
Spanish National Research Council  
(CSIC), Spain

## REVIEWED BY

René Reijer Wijngaard,  
Utrecht University, Netherlands  
Shuai Hu,  
Chinese Academy of Sciences (CAS), China

## \*CORRESPONDENCE

Yanyan Zhao,  
✉ Zhaoyanyan@ouc.edu.cn

RECEIVED 09 September 2024

ACCEPTED 09 December 2024

PUBLISHED 03 January 2025

## CITATION

Yang J, Zhang G, Zhao Y, Zhang Z, Liu S,  
Wei H, Guo X, Cao G, Yang L, Zhang Y and Li S  
(2025) Asynchronous variation in the  
holocene asian monsoon recorded by marine  
sediments and its implication.  
*Front. Earth Sci.* 12:1493790.  
doi: 10.3389/feart.2024.1493790

## COPYRIGHT

© 2025 Yang, Zhang, Zhao, Zhang, Liu, Wei,  
Guo, Cao, Yang, Zhang and Li. This is an  
open-access article distributed under the  
terms of the [Creative Commons Attribution  
License \(CC BY\)](https://creativecommons.org/licenses/by/4.0/). The use, distribution or  
reproduction in other forums is permitted,  
provided the original author(s) and the  
copyright owner(s) are credited and that the  
original publication in this journal is cited, in  
accordance with accepted academic practice.  
No use, distribution or reproduction is  
permitted which does not comply with  
these terms.

# Asynchronous variation in the holocene asian monsoon recorded by marine sediments and its implication

Jun Yang<sup>1</sup>, Guanglu Zhang<sup>1</sup>, Yanyan Zhao<sup>1,2\*</sup>, Zhishun Zhang<sup>1</sup>,  
Sheng Liu<sup>1</sup>, Haotian Wei<sup>1</sup>, Xiaoqiang Guo<sup>1</sup>, Guangyao Cao<sup>1</sup>,  
Lei Yang<sup>1</sup>, Yaru Zhang<sup>1</sup> and Sanzhong Li<sup>1,2</sup>

<sup>1</sup>Key Lab of Submarine Geosciences and Prospecting Techniques, Frontiers Science Center for Deep Ocean Multispheres and Earth System, MOE and College of Marine Geosciences, Ocean University of China, Qingdao, Shandong, China, <sup>2</sup>Laboratory for Marine Mineral Resources, National Laboratory for Marine Science and Technology (Qingdao), Qingdao, Shandong, China

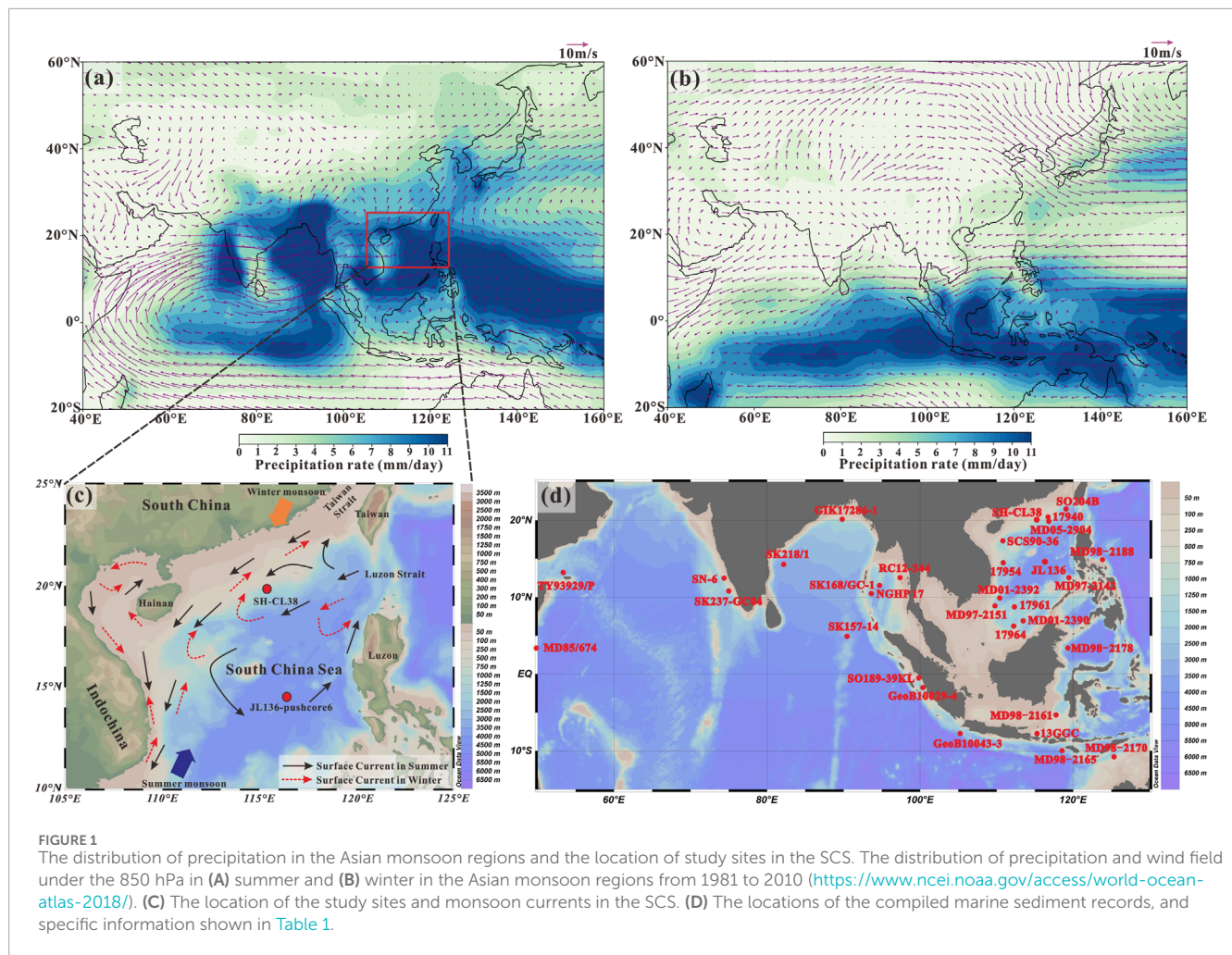
The long-term evolution of climate during the Holocene remains controversial, as proxy and model data, and multiple proxies, show diverging temperature trends between the different reconstructions. Here, we compile sea surface temperature (SST) from multiple marine sediment records in the South China Sea (SCS) and Indo-Pacific over the Holocene, which reveal a phase difference in the precession band of different marine sediment records. Peak identification was performed on the data from each site, and the sea surface temperature anomalies (SSTA) was simply divided into two modes, the Early Holocene (EH-peak) and Middle Holocene (MH-peak), based on the timing of the first maximum peak, using 9 ka as the boundary. The phase difference between the two modes is ~3 ka in the precession band. We suggest that the phase difference corresponds to the shifts in the mean latitudinal position of the Intertropical Convergence Zone (ITCZ) driven by the Northern Hemisphere Summer Insolation (NHSI). Two modes indicate the warming of the SSTA during the late Holocene, which may be attributed to rising  $p\text{CO}_2$ , a strengthening El Niño, and a weakening of the East Asian winter monsoon (EAWM). Furthermore, we observe a partial overlap between the site distribution of the MH-peak and the modern monsoon precipitation domains, which may indicate the shift in the mean latitudinal position of the ITCZ and the dynamics of the monsoon precipitation domains.

## KEYWORDS

holocene, asian monsoon, ITCZ, NHSI, monsoon precipitation domains

## 1 Introduction

The Asian Summer Monsoon (ASM) is a vast system of overturning atmospheric circulation and plays a significant role in the global hydrologic and energy cycles, which consists of two subsystems: the East Asian Summer Monsoon (EASM) and the Indian Summer Monsoon (ISM) (An et al., 2000; Cheng et al., 2021). The ocean has a large heating capacity compared to the continent (Wu et al., 2012). In summer, the Asian continents warm faster than the adjacent oceans, producing an atmospheric



pressure gradient between the ocean and the continent. As a result, warm air carries moisture towards the continent (Figure 1A). In winter, the continents cool faster than the ocean so that the cold and dry air originating from the Siberian high blows from the continent to the ocean (Figure 1B). The ASM system can influence the life and production activities of 60% of the global population (Zhong et al., 2014). Therefore, it is essential to understand the evolution of the monsoon over the geological history.

The Holocene is the major period of human survival and development, whose monsoon climate evolution is crucial to predict the future climate changes. In this way, the research of Holocene monsoon is important. However, the long-term evolution of climate during the Holocene remains controversial, because of often divergent conclusions between multiple proxies and model data, for example, the different temperature trends (Affolter et al., 2019; Baker et al., 2017; Marsicek et al., 2018; Stott et al., 2004). suggests a decreasing trend in temperature over the last 10 ka based on the sediment core records of the western Pacific. In contrast, Marsicek et al. (2018) indicates a warming trend in Holocene temperature based on simulated reconstruction. The main controversies focus on (1) Climate models and pollen-inferred temperature reconstructions showing evidence for lower temperatures during the early Holocene and continuous warming

until the late Holocene in the Northern Hemisphere (Liu et al., 2014b; Marsicek et al., 2018), which challenge previous assumptions of an early to middle Holocene Thermal Maximum (10–6 ka) (Dykoski et al., 2005; Rashid et al., 2007; Selvaraj et al., 2007). (2) The significant phase differences (6–8 ka) in the precession band of Asian monsoon records, observed in a wide range of records varying from marine sediment cores to speleothem  $\delta^{18}O$  records over the Asian continent (Cheng et al., 2021; Clemens et al., 2008). The Asian summer monsoon (ASM) records from the Arabian Sea and other oceans surrounding the Asian continent show a significant lag of  $8 \pm 1$  ka to Northern Hemisphere summer insolation (NHSI) (Clemens et al., 2008; 2010), whereas the Asian cave  $\delta^{18}O$  records lag the NHSI by only  $\sim 2$  ka (Cheng et al., 2016; Cheng et al., 2021). The potential explanations for the asynchronous evolution of the Holocene climate records include underrepresentation of proxies in earlier temperature reconstructions (Marsicek et al., 2018), regional cooling effects related to the remnant ice sheets in the early Holocene (Baker et al., 2017), incomplete forcing or insufficiently sensitive feedbacks of climate model simulations (Liu et al., 2018; Zhang et al., 2018), and seasonal biases between marine records (Liu et al., 2014b; Marsicek et al., 2018). However, the ultimate causes of the asynchronous temperature variations in the Holocene conundrum remain ambiguous.

In order to further understand the asynchronous changes in Holocene temperatures and to provide new insights into solving Holocene conundrum, we estimated sea surface temperature (SST) in the northern and southern South China Sea (SCS) based on the Mg/Ca ratios of planktonic foraminifera shells. Additionally, we compiled more than 30 marine sediment records in the SCS and Indo-Pacific. We compare the compiled results with other Asian monsoon records, expecting to further understand the spatio-temporal distribution characteristics of asynchronous evolution of marine sediment records in the Asian monsoon regions during the Holocene and its implications.

## 2 Materials and methods

Two sediment cores, SH-CL38 (19.9°N, 115.3°E, water depth 1,288 m) and JL136-pushcore6 (14°58.69'N, 116°32.58'E, water depth 2,500 m), were recovered from the northern and central SCS, respectively, during the HYSH201805 cruise and “Jiaolong” 136th dive expedition (Figure 1C). The upper 100 cm of SH-CL38 sediment was described and sampled at 2 cm intervals. However, we only get 31 sediment samples because some samples have been lost in the previous studies, including 0–4 cm, 6–8 cm, 12–14 cm, 22–24 cm, 32–34 cm, 36–38 cm, 42–44 cm, 50–62 cm, 66–70 cm, 72–74 cm, 82–84 cm, 90–92 cm, 96–98 cm. But this does not affect our explanation in this study. The sediments of SH-CL38 primarily consist of silt and clay, with low sand proportion. The core JL136-pushcore6 was described and sampled at 1 cm intervals, resulting in 29 sediment samples. The sediments of the core JL136-pushcore6 mainly consist of gray silty clay with abundant foraminifera. We have further compiled 31 marine sediment records from the Asian monsoon regions to trace the monsoon evolution (Figure 1D; Table 1).

### 2.1 Age models

Accelerator mass spectrometry (Beta Lab, United States)  $^{14}\text{C}$  dates were obtained on mixed planktonic species (*G. ruber* and *G. sacculifer*), and calibrated to calendar age using CALIB8.2 software (Heaton et al., 2020). Based on the Marine Reservoir Correction Database (<http://intcal.qub.ac.uk/calib/>), the regional reservoir correction ages ( $\Delta \pm R$ ) obtained from the five nearby sites were  $5 \pm 52$  years (JL136) and  $-94 \pm 59$  years (SH-CL38), respectively (Yang et al., 2023). The AMS  $^{14}\text{C}$  calibrated results with a  $2\sigma$  error range can offer precise age control for sediment cores. The chronology was based on the results from Bayesian modeling employing the Oxcal program. Subsequently, the Poisson-process deposition model was applied to obtain the age-depth model (Table 2) (Bronk, 2009; Ramsey and Lee, 2013). Temporal intervals between the samples of cores JL136-pushcore6 and SH-CL38 is  $\sim 350$  and  $\sim 280$  years, respectively. The results indicate that the age range of cores JL136-pushcore6 and SH-CL38 is 2.1–12.8 ka, and 1.5–14.4, respectively. In this study, we focus exclusively on Holocene sediment samples for testing and analysis (Figure 2).

### 2.2 Mg/ca ratios

The relationship between calcification temperatures and Mg/Ca ratios in shells (or tests) of foraminifera has been quantified from core-top, sediment trap, and culture studies, resulting in paleotemperature calibration equations (Dekens et al., 2002; Anand et al., 2003; Tierney et al., 2019). This relationship has long been used in paleoclimate reconstructions (Brown and Elderfield, 1996; Nürnberg et al., 1996; Rosenthal et al., 1997; Steinke et al., 2006; Yin et al., 2021; Yang et al., 2023). Typically, SST reconstructions generated from Mg/Ca ratios are obtained from monospecific aggregates of 5–30 shells by the solution method using ICP-AES or ICP-OES (Marchitto, 2006; Rongstad et al., 2017; Groeneveld et al., 2019). In recent years, with the development of testing techniques, Laser ablation inductively coupled plasma mass spectrometry (LA-ICP-MS) is becoming a widespread technique for analyzing elemental ratios in foraminifera calcite (Eggins et al., 2003; Sadekov et al., 2009; Sadekov et al., 2010; Fehrenbacher et al., 2015). Inter-method comparisons studies comparing average Mg/Ca ratios obtained from LA-ICPMS on discrete chambers and ICP-AES or ICP-OES analysis of complete shells have found that population mean values are consistent (Groeneveld et al., 2008; Sadekov et al., 2009; Jochum et al., 2019; Rustic et al., 2021). Thus, the analysis of Mg/Ca ratios from individual foraminifera using LA-ICP-MS has opened new dimensions in paleoclimate reconstructions, allowing for paleoceanographic reconstruction of oceanic variability (Ford et al., 2015; White et al., 2018; Rustic et al., 2020).

A suitable number (not less than 6) tests of *G. ruber* (s.s.) with sizes ranging from 250 to 350  $\mu\text{m}$  were extracted from each sample of core SH-CL38. In order to avoid the influence of debris materials on the test results, a gentle ultrasonic pre-treatment of the samples with reagent-grade methanol solution was performed with reference to the method of Vetter et al. (2013). The cleaned samples were oven-dried at 40°C. This analysis was carried out at the Key Lab of Submarine Geosciences and Prospecting Techniques, Ocean University of China. Each sample was fixed on a glass slide using carbon tape to facilitate the measurement of laser ablation inductively coupled plasma mass spectrometry (LA-ICP-MS). Six erosion points were selected for each foraminifera, with 2 points in each chamber (Figure 2). A high-resolution LA-ICP-MS technique using a pulsed ArF excimer laser ( $k = 193$  nm) coupled to a NexlOn 2000 inductively coupled plasma mass spectrometer (ICP-MS) was employed to generate depth profiles across test walls. Prior to the analysis of the different spot sizes and laser intensities, multiple measurements of the foraminiferal test were conducted to obtain the optimal signal. The optimal laser beam spot diameter was fixed at 32  $\mu\text{m}$ , the energy density at 4 J/cm<sup>2</sup>, and the erosion frequency at 5 Hz (laser shots per second). The total design time of a single point was 105 s, of which the air-carrying blank was 25 s, the erosion time was 40 s, and the washing time was 40 s.  $^{43}\text{Ca}$  was used as an internal standard since all the measurements in this study were obtained from foraminiferal calcite.  $^{44}\text{Ca}$  was used as monitor to ensure consistency, while  $^{27}\text{Al}$  and  $^{55}\text{Mn}$  were used to evaluate the surface contamination and prevent penetrating shells (which produces a diagnostic signal at  $^{27}\text{Al}$ ). In this way, any ratios of Al/Ca >0.10 mmol/mol and Mn/Ca >0.25 mmol/mol were excluded from the average dataset because the contamination always results in higher Al/Ca and Mn/Ca ratios. The NIST SRM

TABLE 1 The information from the marine sediment cores and Asian cave records was used in this study.

Site/Cave	Latitude (N)	Longitude (E)	Water depth (m)	References
SCS9036	17°35.8'	111°17.4'	2050	Huang et al. (1997)
GIK17964	06°09.5'	112°12.8'	1,556	Steinke et al. (2008)
GIK17961	08°30.4'	112°19.9'	1968	Wang et al. (1999)
GIK18252	09°14'	109°23'	1,273	Kienast et al. (2001)
MD01-2,390	06°38.1'	113°24.6'	1,545	Steinke et al. (2008)
MD01-2,392	09°51.1'	110°12.6'	1966	Huang J et al. (2011)
MD97-2,142	12°24.7'	119°16.7'	1,557	Chen et al. (2003)
MD97-2,151	08°43.7'	109°52.2'	1,598	Huang et al. (2002)
MD98-2,178	03°37.2'	118°54'	1984	Fan et al. (2013)
MD98-2,188	14°49.2'	123°29.4'	730	Lin et al. (2006)
SK157-14	05°11'	90°05'	3,306	Raza et al. (2017)
SK168/GC01	11°42.4'	94°29.6'	2064	Gebregiorgis et al. (2016)
SK237/GC04	10°58.6'	74°59.4'	1,245	Saraswat et al. (2013)
GeoB10029-4	-01°58.6'	100°46.1'	964	Mohtadi et al. (2010)
SO189-39 KL	-00°47'	99°54'	517	Mohtadi et al. (2014)
NGHP 17	10°45.2'	93°06.7'	1,356	Gebregiorgis et al. (2018)
MD85674	03°06.1'	50°15.6'	4,875	Bard et al. (1997)
TY93929/P	13°02'	53°05'	2,490	Rostek et al. (1997)
GIK17286-1	19°44.6'	89°52.7'	1,428	Lauterbach et al. (2020)
GIK17938	19°47.2'	117°32.3'	2,840	Chen et al. (1999)
GIK17940	20°07'	117°23'	1728	Huang et al. (2009)
MD05-2,904	19°27.3'	116°15.2'	2066	He et al. (2008)
MD98-2,161	-05°12.6'	117°28.8'	1,185	Fan et al. (2013)
MD98-2,165	-09°39'	118°20.4'	2,100	Levi et al. (2007)
MD98-2,170	-10°21.3'	125°23.3'	832	Stott et al. (2007)
SO50-31 KL	18°45.3'	115°52.4'	3,360	Zhao et al. (2006)
SO204B	21°13'	118°05'	1822	Yang et al. (2019b)
GeoB10043-3	-07°18.6'	105°03.5'	2,171	Setiawan et al. (2015)
13 GG C	-07°14.4'	115°12'	594	Linsley et al. (2010)
SN06	12°29.2'	74°07.8'	589	Tiwari et al. (2015)
RC12-344	12°27.6'	96°02.4'	2,140	Rashid et al. (2007)
SK218/1	14°02'	82°00'	3,307	Govil and Divakar (2011)

(Continued on the following page)

TABLE 1 (Continued) The information from the marine sediment cores and Asian cave records was used in this study.

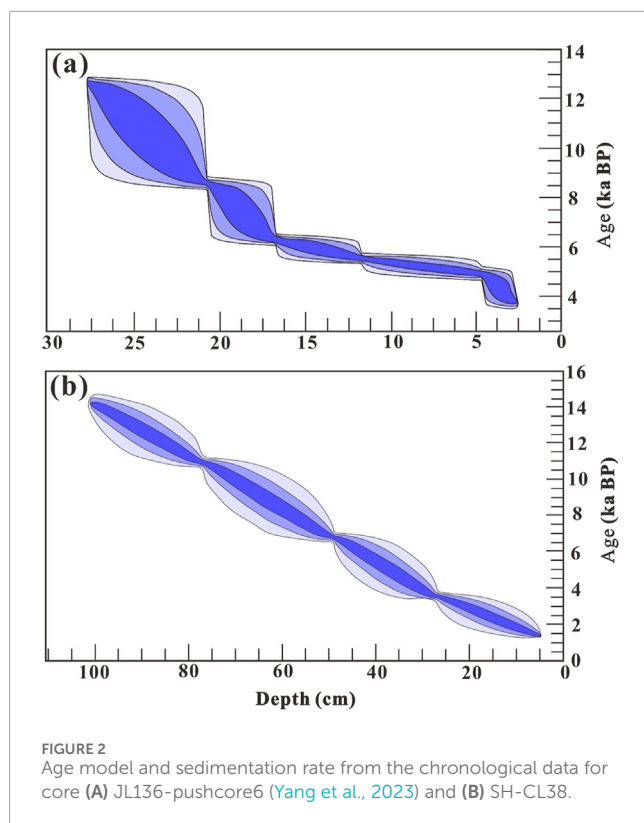
Site/Cave	Latitude (N)	Longitude (E)	Water depth (m)	References
GHE27L	19°51'	115°20.4'	1,533	Yang et al. (2019b)
SH-CL38	19°54'	115°18'	1,288	This study
JL136-pushcore6	14°58.69'	116°32.58'	2,500	Yang et al. (2023)
Jiuxian	38°24'	113°48'	--	Cai et al. (2010)
Sanbao	31°00'	110°36'	--	Cheng et al. (2016)
Heshang	30°27'	110°25'	--	Hu et al. (2008)
Heifeng	29°40'	106°17'	--	Yang et al. (2019a)
Dongge	25°17'	108°5'	--	Dykoski et al. (2005)
Lianhua	38°24'	113°48'	--	Dong et al. (2015)
Mawmluh	25°5'	91°2'	--	Dutt et al. (2015)
Bukit Assam	4°17'	114°55'	--	Carolin et al. (2013)
Tangga	-0°19'	100°43'	--	Wurtzel et al. (2018)
Klang	8°18'	98°42'	--	Chawchai et al. (2021)
Gempa Bumi	-5°18'	120°42'	--	Krause et al. (2019)

TABLE 2 AMS-<sup>14</sup>C ages and calendar ages of core SH-CL38 and JL136-pushcore6 (Yang et al., 2023).

Sample ID	Sample depth (cm)	Materials	AMS <sup>14</sup> C age (yr BP)	Calendar age (cal. yr BP)	2 sigma age (cal. yr BP)
SH-CL38	4–6	<i>G. ruber</i> (s.s.)	2070 ± 25	1,478	1,272–1,684
	26–28	<i>G. ruber</i> (s.s.)	3,790 ± 30	3,595	3,358–3,832
	48–50	<i>G. ruber</i> (s.s.)	6,555 ± 40	6,856	6,581–7,132
	76–78	<i>G. ruber</i> (s.s.)	10,070 ± 30	10,948	10,695–11,202
	100–102	<i>G. ruber</i> (s.s.)	12,745 ± 45	14,357	13,922–14,792
JL136-pushcore6	3–4	<i>G. ruber</i> (s.s.) + <i>G. sacculifer</i>	4,105 ± 30	3,982	3,707–4,258
	5–6	<i>G. ruber</i> (s.s.)	5,045 ± 25	5,149	4,879–5,420
	12–13	<i>G. ruber</i> (s.s.)	5,560 ± 25	5,758	5,543–5,973
	17–18	<i>G. ruber</i> (s.s.)	6,260 ± 30	6,512	6,280–6,744
	21–22	<i>G. ruber</i> (s.s.)	8,430 ± 30	8,808	8,549–9,067
	27–28	<i>G. ruber</i> (s.s.)	11,550 ± 40	12,877	12,656–13,098

610 and 614 soda-lime glass standard were employed to quantify the internal variability within each group and assess the relative differences among groups. In this study, two measurements on per chamber were conducted to calculate the average Mg/Ca ratio for

each foraminifera. The mean Mg/Ca variability in the chamber was about ±0.16 mmol/mol. Finally, the mean Mg/Ca variability from all measurements (at least 30 measurements in one sample) was determined of ±0.37 mmol/mol.



For core JL136-pushcore6, Mg/Ca ratios were analyzed using Arian 720ES ICP-OES in the Key Laboratory of Ocean and Marginal Sea Geology, SCS Institute of Oceanology Chinese Academy of Science. Specific pre-treatment and test parameters are described in Yang et al. (2023).

We converted Mg/Ca ratios to SST using a calibration,  $\text{Mg/Ca (mmol/mol)} = 0.38\text{exp}[0.09\text{SST (}^\circ\text{C)}]$  (Dekens et al., 2002). Testing of Mg/Ca ratios and reconstructed SST can be found in Supplementary Table S1.

## 2.3 Compilation of marine sediment records

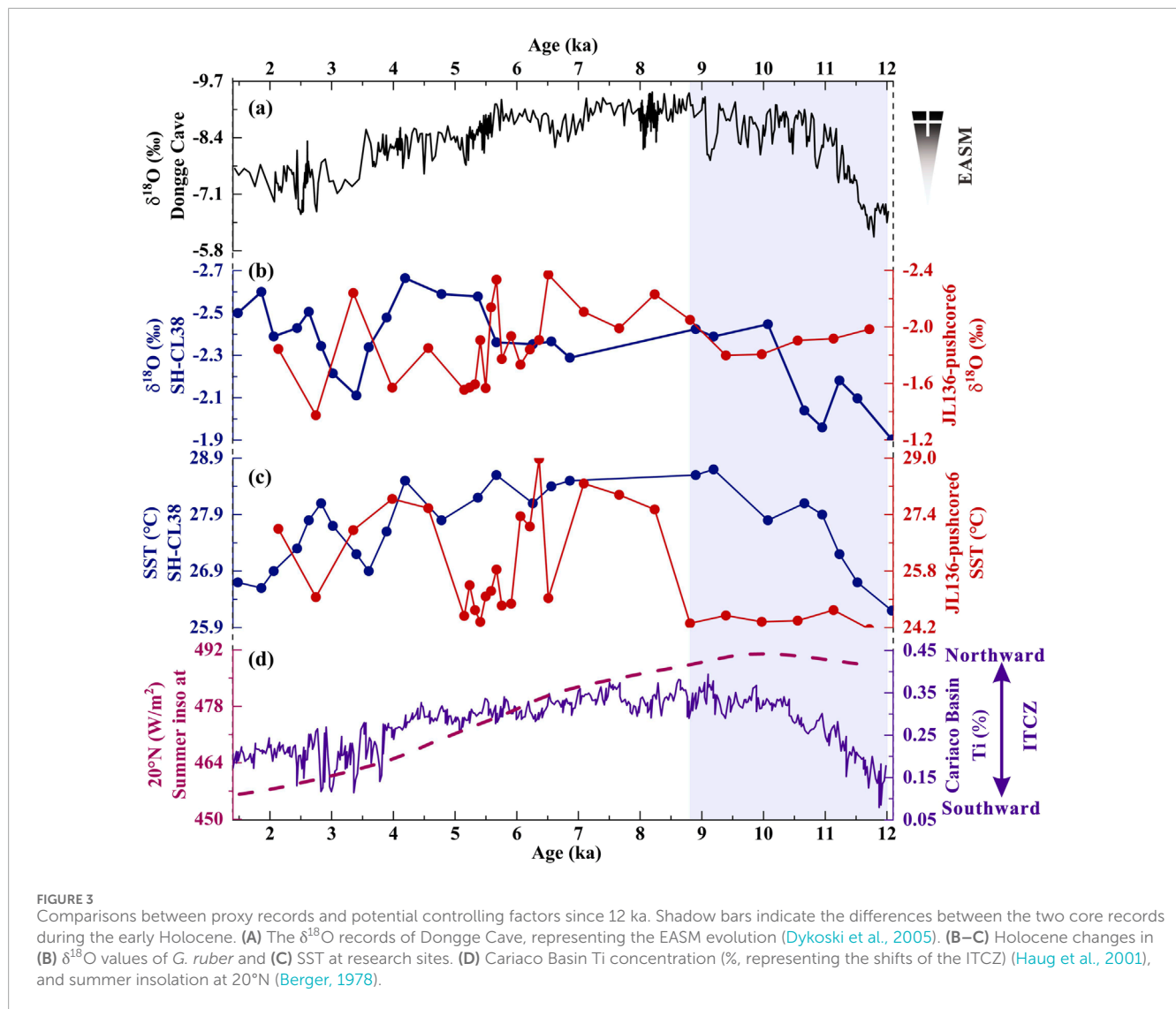
There are a lot of studies on the evolution of the Monsoon evolution (Affolter et al., 2019; Böll et al., 2015; Lo et al., 2013; Raza et al., 2017; Yang et al., 2023; Yin et al., 2021). However, the reconstructed SST values in the studies can be affected by possible inter-laboratory and inter-calibration biases and different cleaning protocols (Dang et al., 2020), which result in the difficulties to reach a consensus. To minimize this biases and differences, we calculated the SST anomalies relative to the average value of each temperature record over 6 to 10 ka, which is denoted as the sea surface temperature anomalies (SSTA) (Supplementary Figure S1). Given the differences between the resolution of samples from different sites, we have selected to bin the SSTA into 500-year non-overlapping bins (Supplementary Figure S2) (Linsley et al., 2010). This composite reconstruction is based on binning of the original data and not interpolation, and the treatment of the data is referenced from Linsley et al. (2010).

## 3 Results and discussion

### 3.1 Asynchronous evolution of the SCS sediment records

In the northern SCS, the results show that the SST range from 26.2°C to 28.7°C at the site SH-CL38 over the last 12 ka, with a rapid increase from 26.2°C to 27.9°C during 12–11 ka. Then, from 11 to 5.4 ka, higher SST values were observed, with an average of 28.3°C. After 5.4 ka, there was a gradual decline in SST, with a mean value of 27.5°C (Figure 3). The general trend shows similarity with the reconstructed SST using alkenone, planktonic foraminiferal  $\delta^{18}\text{O}$  values, and Mg/Ca ratios at 17,940 (Wang et al., 1999), SCS90-36 (Huang et al., 1997), ODP1144 (Wei et al., 2007), and KNG5 (Huang E et al., 2011) sites in the northern SCS. In addition, these records have a similar trend to the stalagmite  $\delta^{18}\text{O}$  values of Dongge Cave, with a rapid warming in the early Holocene, followed by a warmer and wetter middle Holocene, and gradual cooling in the Late Holocene (Cheng et al., 2019; Dong et al., 2010). In contrast, in the central SCS, the SST ranges from 24.2°C to 29.0°C at the site of JL136-pushcore6. The SST (24.2–24.7°C) was low from 11.7 to 8.8 ka, followed by rapid increase from 24.3°C to 29.0°C during 8.8–6.1 ka and a gradual decrease during the late Holocene (after ~6.1 ka). This SST trend indicates that the sediment record in the central SCS did not significantly warm during the early Holocene and rapidly warmed in the middle Holocene. until the mid-Holocene. The warming observed in the sediment record of the central SCS lags that of the northern SCS by ~3 ka (Figure 3).

The evolution trend of the northern SCS sediment records is consistent with the stalagmites  $\delta^{18}\text{O}$  values of Dongge Cave (Cheng et al., 2019; Dong et al., 2010; Dykoski et al., 2005) (Figure 3A). The stalagmites  $\delta^{18}\text{O}$  values were interpreted as a comprehensive representation of the entire water vapor transport process, reflecting the intensity of the EASM across the continent (Cheng et al., 2019; Cheng et al., 2021; Ruan et al., 2019). Thus, the northern SCS sediment records reflect EASM variability (Oppo and Sun, 2005; Yin et al., 2021; Yokoyama et al., 2011). The EASM intensity variations inferred by the stalagmites  $\delta^{18}\text{O}$  values are consistent with NHSI changes, revealing that the EASM is mainly driven by insolation forcing on orbital timescale (Cheng et al., 2019; Wang et al., 2001). The NHSI changes along with the movement of the mean latitude of the Intertropical Convergence Zone (ITCZ) (Cheng et al., 2019; Dong et al., 2018; Fleitmann et al., 2007). During the high NHSI period, the overall northward shifts of the ITCZ is accompanied by a weakened Northern Hemisphere Hadley cell and a strengthened Southern Hemisphere cell, increasing cross-equatorial airflows (Chiang and Friedman, 2012; Du et al., 2021). This results in an enhanced sea-land temperature and pressure gradient, ultimately leading to a strengthening of the EASM and an increase in monsoon precipitation, whereas the opposite effect is observed during the low NHSI (Cheng et al., 2021; Du et al., 2021). Therefore, the rapid warming recorded in the northern SCS during the early Holocene was influenced by an enhanced EASM with high NHSI forcing (Chiang et al., 2015; Kong et al., 2017). The simulation results of the precipitation differences between high NHSI minus low NHSI show that the southerly monsoon over East Asia enhanced at high NHSI along with the enhancement of the western Pacific Subtropical High (Bosmans et al., 2018). This has resulted in the movement of the main precipitation belts deeper into the continent and a decrease



in oceanic precipitation around the southeastern-south of the Asian continent (Bosmans et al., 2018; Huang et al., 2020; Lee et al., 2019; Wang et al., 2016). The northern SCS continuously warmed, with an increasing monsoon rainfall during the early Holocene (Cheng et al., 2019; Dong et al., 2018; Huang et al., 2016). Geographically, the central SCS is closer to the equator, but further away from Asian continents compared to the northern SCS. The asynchronous SST evolution of the Early Holocene in the northern and central SCS records may be a response to the northward shift of the ITCZ forced by the high NHSI (Bosmans et al., 2018; Kong et al., 2017; Zhang et al., 2021). During the middle Holocene, warm and humid Holocene optimums were recorded by cores from both northern and central SCS (An et al., 2000; Zhou et al., 2016). The warm and humid Middle Holocene optimum is also recorded by other proxies in the Asian monsoon region, such as lake sediments (Jia et al., 2015; Rao et al., 2016), Asian cave stalagmite  $\delta^{18}\text{O}$  records (Dong et al., 2018), and loess-paleosol records (Jia et al., 2021; Wang et al., 2014), which may be attributed to the variation of the NHSI. As the NHSI gradually decreases, the ITCZ begins to retreat southwards. During this period, the tropical monsoon trough and the main precipitation belts shift southward, leading to a decrease in total rainfall at the northern edge of the Asian monsoon domain, while the

overall climate in the SCS region is warm and humid (Anwar et al., 2018; Fleitmann et al., 2007; Jia et al., 2021; Zhou et al., 2016).

### 3.2 The different evolution modes of holocene climate

We present a compilation of more than 30 marine sediment records from the Asian monsoon regions to further understand the asynchronous variation of the Asian monsoon records in the precession band and its implications (Table 1). We identified peaks in the data from each station and simply divided the SSTA into two modes, based on the timing of the first maximum peak (Supplementary Figure S3). Because the first rapid warming occurred mainly in the Early and Middle Holocene, we use 9 ka as the boundary and divide it into two modes, the Early Holocene peak (EH-peak) and the Middle Holocene peak (MH-peak). To more clearly describe the patterns of the temperature variation, we calculated its mean SSTA values (Figure 4). The EH-peak mode shows that the mean SSTA continuously warms by  $\sim 0.9^\circ\text{C}$  since  $\sim 12$  to 10.5 ka, followed by a stable period during 10.5–5 ka, with warms by  $\sim 0.3^\circ\text{C}$  after  $\sim 5$  ka. The

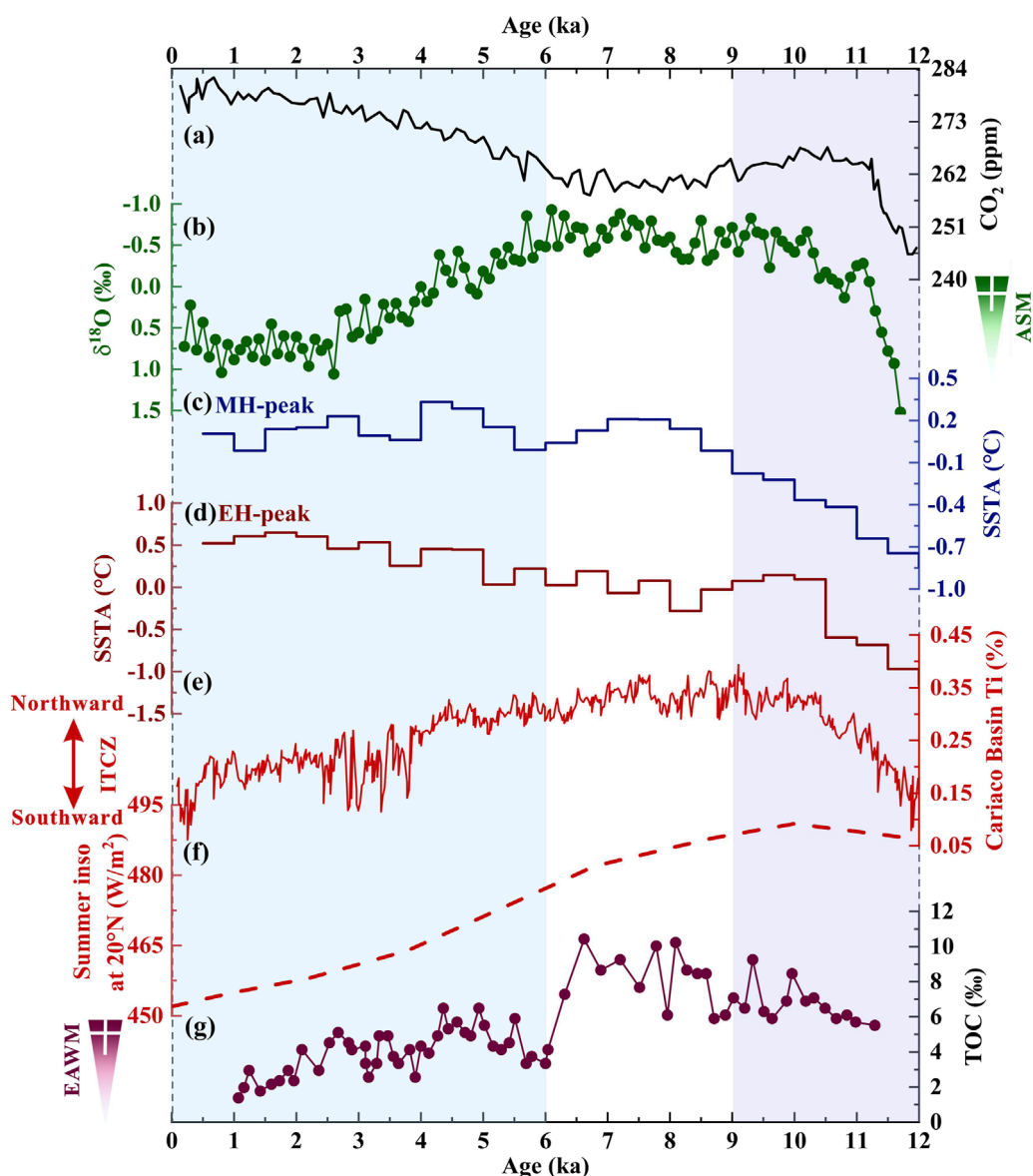


**FIGURE 4** Comparisons between proxy records and potential controlling factors during the Holocene. Purple bars indicate differences between the two modes during the early Holocene. Blue bars indicate changes in the two modes during the Late Holocene. **(A)** Holocene changes in CO<sub>2</sub> concentration (Lüthi et al., 2008). **(B)** The anomalous variation of stalagmite δ<sup>18</sup>O records for several caves in the Asian monsoon regions, representing the ASM evolution (c–d) 500 years non-overlapping binned average SSTA in **(C)** MH-peak mode and **(D)** EH-peak mode. **(E)** Cariaco Basin Ti concentration (%), representing the shifts of the ITCZ (Haug et al., 2001). **(F)** Summer insolation at 20°N (Berger, 1978). **(G)** Total organic carbon (TOC) concentration from the Huguangyan Maar Lake, Guangdong province, regarded as an indicator of the EAWM with high/low values indicating strong/weak EAWM (Jia et al., 2015).

MH-peak mode shows that the first peak of mean SSTA occurs at ~8 ka, which lags the EH-peak model by ~3 ka in the precession band. Then the mean SSTA kept stable after 8 ka (Figure 4).

### 3.3 Potential influence factors on different modes

The long-term evolution of climate during the Holocene remains controversial, because we can get the different temperature trends based on the different reconstruction methods (Affolter et al., 2019).

Stott et al. (2004) found a decrease in SST of 0.5°C in the western tropical Pacific Ocean over the past 10 ka using three sediment cores. Linsley et al. (2010) found a cooling trend during the late Holocene in the western tropical Pacific warm pool by eight sediment cores. Marcott et al. (2013) proposed that the climate kept warming during the early-middle Holocene (11.3–5 ka), with a gradually decreasing temperature in the late Holocene from 73 globally distributed records. However, there are also contrary opinions. The SST reconstructions in the eastern equatorial Pacific and SCS show a gradual warming from the early to late Holocene, and the Mg/Ca-SST of the Northwestern Atlantic also shows a relatively stable or

slightly warming during the Holocene (Leduc et al., 2010). Liu et al. (2014b) suggest that the SST warms from the early Holocene and did not cool until the Little Ice Age (1,300–1,850 AD) based on three climate models, which simulated the global and regional mean temperatures over the Holocene. In addition, the results also show warming from the early Holocene up to ~2 ka by reconstruction of Northern Hemisphere temperatures from sub-fossil pollen in North America and Europe (Marsicek et al., 2018). Our EH-peak and MH-peak modes show an increase trend in SSTA after ~6 ka, which supports the argument of Late Holocene warming (Figure 4) (Leduc et al., 2010; Liu et al., 2014b; Marsicek et al., 2018).

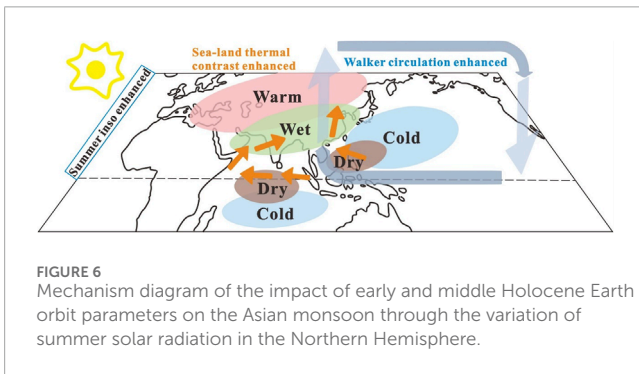
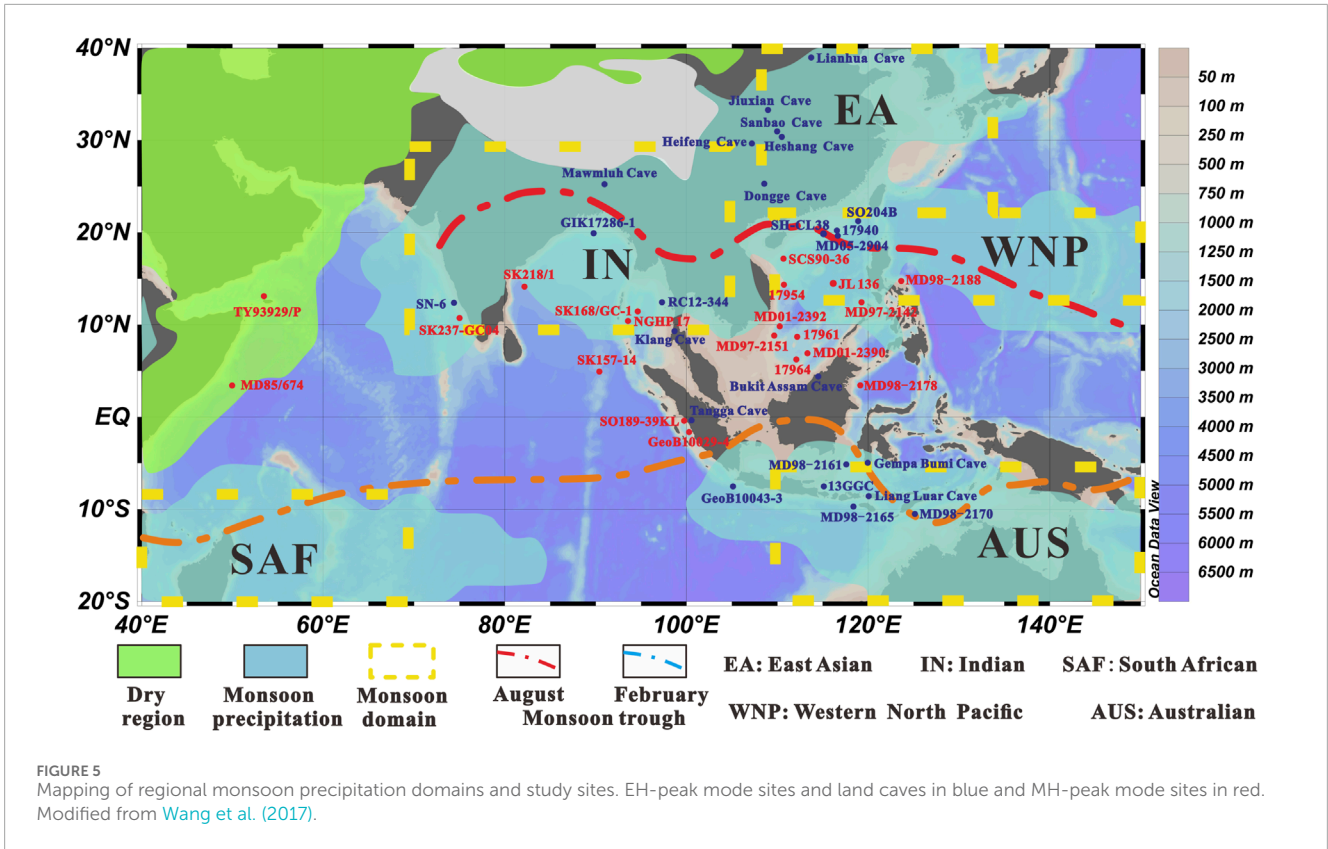
It has been proposed that the monsoon climate is primarily driven by the solar radiation intensity, which can be mainly reflected by NHSI, caused by the Earth's orbital parameters on orbital timescale since the Quaternary (Imbrie et al., 1992). The NHSI reached a Holocene maximum at ~11.5 ka and then decreased, which may controlled the overall trend of the ASM (Laskar et al., 2004). The EH-peak mode is mainly controlled by the NHSI, with a rapidly increase of mean SSTA, which reached the first peak in the early Holocene, and kept relatively stable in the middle Holocene (Figure 4). The MH-peak mode shows that the mean SSTA varied lags the NHSI by ~3 ka. It gradually increased during the early Holocene and reached its first peak in the middle Holocene. The solar radiation variations can cause seasonal migration of the ITCZ (Dong et al., 2010). During the early Holocene, the intensified summer solar radiation in the Northern Hemisphere contributed to an increase in the interhemispheric thermal gradient, which was accompanied by a rapid northward shift of the ITCZ (Chiang and Friedman, 2012). This shift facilitated the transport of more warm water vapor from the Indian Ocean to the Asian Monsoon region, thereby enhancing the EASM and leading to increased monsoon precipitation and warmer temperatures (Chawchai et al., 2021; Fleitmann et al., 2007; Wu et al., 2020). During the middle and late Holocene, the decreasing northern hemisphere summer solar radiation intensity weakens, can lead to the southward shift of the ITCZ and a gradually decreasing ASM intensity (Dong et al., 2010; Fleitmann et al., 2003; Fleitmann et al., 2007).

Both mentioned modes indicate that the mean SSTA warmed during the late Holocene, contrary to the weakening summer monsoon due to the reduction of northern hemisphere summer insolation. This indicates that other factors may influence the SSTA (Huang J et al., 2011; Laskar et al., 2004). Previous studies suggest that SST variations in the Late Holocene were significantly influenced by the East Asian winter monsoon (EAWM) (Kong et al., 2014; Yang et al., 2019b). The EAWM induces strong stirring of seawater, resulting in a net loss of heat from the sea surface to the air, which would lead to a decrease in SST (Chen et al., 1999; Yang et al., 2019b). A weakened EAWM may weaken the mixing of the upper water layer, resulting in a warming of the SST (Yang et al., 2019b). Jia et al. (2015) revealed a weakening of the EAWM from the early to late Holocene, with the most significant transition at ~6 ka, based on the biogeochemical records from Huguang Maar Lake. Kaboth-Bahr et al. (2021b) also revealed a weakening of the winter monsoon from ~5 ka until ~2 ka by stacking marine and terrestrial proxy records. The weakened EAWM was influenced by the enhanced El Niño activity in the late Holocene (Dong et al., 2021). Enhanced El Niño activity suppresses the EAWM through southerly anomalies generated by anticyclonic circulation anomalies

in the western Pacific Ocean (Dong et al., 2021; Huang et al., 2004). The weakened EAWM was accompanied by southeasterly anomalies, which transport warm and humid air from the tropical oceans northward, resulting in increased monsoon humidity and a gradual warming of temperatures (Ma et al., 2018). So, the combination of strengthened El Niño and weakened EAWM causes increased monsoon rainfall and temperatures in southeastern and SCS. In addition, CO<sub>2</sub> as a greenhouse gas has a significant influence on climate change (Wen et al., 2016). The atmospheric CO<sub>2</sub> contents continuously rose since ~6 ka, resulting in the infrared radiation difficulty escape from the atmosphere and lack of heat exchange, leading to a thermal insulation effect and atmospheric warming (Hu et al., 2000; Wen et al., 2016). Observation and model results suggest a negative correlation between atmospheric CO<sub>2</sub> contents and the Asian winter monsoon intensity under global warming conditions (Hori and Ueda, 2006; Kaboth-Bahr et al., 2021b; Li et al., 2019). Therefore, the warming of the mean SSTA during the Late Holocene may have been influenced by the combination of increased CO<sub>2</sub> contents, a strengthened El Niño, and a weakened EAWM.

### 3.4 Implications of the holocene climate mode for the asian monsoon regions

The EH-peak and MH-peak modes have a regular distribution based on the compilation of the sediment records in the different study sites (Figure 5). The EH-peak mode mainly occurred in the oceans surrounding the Asian continent, while the MH-peak mode mainly occurs in the oceans away from the Asian continent (Figure 5). Dong et al. (2010) suggested that shifts in the mean position of the ITCZ control the monsoon intensity throughout the entire low-latitude region of Asia on the orbital timescales based on the Asian cave δ<sup>18</sup>O records. The shift in the mean latitudinal position of the ITCZ are forced by the intensity of the NHSI (Fleitmann et al., 2003; Fleitmann et al., 2007), which reached the Holocene maximum with weak winter insolation intensity during the early Holocene (Laskar et al., 2004). The northern hemisphere is located at perihelion and aphelion in summer and winter, respectively, which can lead to further seasonal contrast in insolation (Wang et al., 2008). This process, in turn, can enhance the sea-land thermal contrast, and eventually increase summer and winter monsoon strength (Wang et al., 2008). In addition, the intensity of summer insolation in the Northern Hemisphere was much stronger than in the Southern Hemisphere during the Early Holocene, which strengthened the cross-equatorial airflows, resulting in a further northward shift in the mean position of the ITCZ (Chawchai et al., 2021; Fleitmann et al., 2007). This transports large amounts of warm water vapor from the Indian Ocean into the Asian monsoon region, resulting in increased monsoon precipitation and temperatures in the interior Asian continent and along the southern coasts (Chawchai et al., 2021; Fleitmann et al., 2007; Wu et al., 2020). Meanwhile, the oceans away from the Asian continent can only accept the relatively less influence of warm and humid air. During the middle Holocene, the NHSI weakened and winter insolation intensity gradually increased, which resulted in a weakening sea-land thermal contrast, and a gradually southward shifting in the mean position of the ITCZ (Zhang et al., 2021). Under this condition, the oceans away from the Asian continent should be strongly influenced by the warm and humid air, which can be observed from the EH-peak and



MH-peak modes (Figure 5). Therefore, the EH-peak and MH-peak modes should be caused by the northern hemisphere solar radiation variability, and the phase differences in the precession band may reflect different aspects of the monsoon dynamics, which is also proposed by Cheng et al. (2019) and Dong et al. (2010).

According to the modern definition of monsoon climate, precipitation becomes an important limited factor in the delineation of the monsoon domains (Wang et al., 2017). The Asian monsoon regions mainly contain the Indian, the western North Pacific, and the East Asian monsoon precipitation domains (Yim et al., 2014). According to the distribution of the modern monsoon precipitation domains, the EH-peak sites are located within the monsoon precipitation domains, while the MH-peak sites are mainly outside the precipitation domains, with parts of the sites at the edge of the precipitation domains (Figure 5) (Yim et al., 2014). These distributions are mainly related to the seasonal

migration of the ITCZ (Fleitmann et al., 2007; Wang et al., 2017), accompanied by the migration of the latitudinal zone of wind convergence and precipitation, which determines the onset, duration, and termination of the rainy season in the tropics and subtropics (Fleitmann et al., 2007). Kaboth-Bahr et al. (2021a) inferred that the mean position of the ITCZ has shifted southward or northward 10°–15° since the 20 ka from its current position based on the variations of terrigenous input fluxes into the northern SCS. The shift in the mean position of the ITCZ are accompanied by monsoon rainfall variability (Fleitmann et al., 2007). Liu et al. (2014a) modeled the precipitation difference between middle Holocene (6 ka) and late Holocene (1 ka) and proposed that the precipitation was strengthened in the Asian continent but weakened in the oceans away from the Asian continent compared to the present, revealing that the mean position of the ITCZ is more northerly than present in the middle Holocene. During the early Holocene, the NHSI experienced a Holocene maximum, with strong insolation seasonal contrasts and enhanced sea-land thermal contrasts, which led to a further amplified the northward shift in the mean position of the ITCZ, and the monsoon precipitation domains was more northerly than in the present (Fleitmann et al., 2007; Wang et al., 2008). In addition, the westward shift of the tropical Pacific Walker circulation also further strengthens the Asian monsoon, resulting in a warmer and wetter climate on the Asian continent, while oceans around the Asian continental are also affected (Figure 6) (Tian et al., 2018; Wang et al., 2020). The distributional characteristics of the EH-peak and MH-peak mode sites coincide with the northward shift in the mean position of the ITCZ during the early Holocene. The partial MH-peak sites

located in the modern monsoon precipitation domains indicate that the mean position of the ITCZ was further north compared to the present  $\sim 24^\circ\text{N}$  during the early Holocene (Kaboth-Bahr et al., 2021a). During this period, the Asian continent and the southern coastal areas are located within the monsoon precipitation domain, where the monsoon precipitation and temperature increase. In contrast, the ocean areas far from the continents had relatively cooler temperatures and less monsoon precipitation. In the Middle and Late Holocene, as the NHTSI decreased, the ITCZ gradually shifted southward, accompanied by a southward shift in the monsoon precipitation domain (Chawchai et al., 2021; Fleitmann et al., 2007). This resulted in increased monsoon precipitation and temperature at some oceanic areas far from the continent. The partial overlap between the site distribution of the MH-peak and the modern monsoon precipitation domains seems to corroborate the latitudinal shift of the ITCZ. Therefore, we suggest that the difference between the two modes, may indicate a change in the mean latitudinal position of the ITCZ and the dynamics of the monsoon precipitation watershed.

## 4 Conclusion

We analyze the core sediment records from the northern and central SCS and find that there are significant phase differences not only between the marine sediment records and the Asian cave  $\delta^{18}\text{O}$  records in the precession band but also between the marine sediment records. We re-analyze SST data from marine sediment records in the Asian monsoon regions and establish two modes, EH-peak and MH-peak. The results show that the mean SSTA peak of the MH-peak mode lags the EH-peak mode by  $\sim 3$  ka in the precession band. On the Holocene long-term trend, the two climate modes respond to the northern hemisphere solar radiation variability, and the phase differences in the precession band may reflect different aspects of the monsoon dynamics. Two modes indicate warming of the SSTA during the late Holocene, which may be attributed to rising  $p\text{CO}_2$ , a strengthening El Niño, and a weakening of the EAWM. In addition, the distribution of the two Holocene modes sites responds to the distribution of monsoon precipitation domains and is implication the dynamics of the monsoon precipitation domains.

## Data availability statement

All relevant data is contained within the article: The original contributions presented in the study are included in the article/Supplementary Material.

## Author contributions

JY Writing–original draft, Writing–review and editing. GZ: Writing–review and editing. YnZ: Writing–review and editing. ZZ:

## References

Affolter, S., Häuselmann, A., Fleitmann, D., Edwards, R. L., Cheng, H., and Leuenberger, M. (2019). Central Europe temperature constrained by speleothem

Formal Analysis, Methodology, Writing–review and editing. SL: Formal Analysis, Methodology, Writing–review and editing. HW: Formal Analysis, Methodology, Writing–review and editing. XG: Formal Analysis, Methodology, Writing–review and editing. GC: Formal Analysis, Methodology, Writing–review and editing. LY: Formal Analysis, Methodology, Writing–review and editing. YrZ: Formal Analysis, Methodology, Writing–review and editing. SL: Writing–review and editing.

## Funding

The author(s) declare that financial support was received for the research, authorship, and/or publication of this article. This project was funded by the National Natural Science Foundation of China (No. 41873006), the Natural Science Foundation of Shandong Province (ZR2023MD092).

## Acknowledgments

We are sincerely grateful to Nan Wang, Yang Zhang in the Key Lab of Submarine Geosciences and Prospecting Techniques, Ocean University of China for their helping with elemental analysis.

## Conflict of interest

The authors declare that the research was conducted in the absence of any commercial or financial relationships that could be construed as a potential conflict of interest.

## Publisher's note

All claims expressed in this article are solely those of the authors and do not necessarily represent those of their affiliated organizations, or those of the publisher, the editors and the reviewers. Any product that may be evaluated in this article, or claim that may be made by its manufacturer, is not guaranteed or endorsed by the publisher.

## Supplementary material

The Supplementary Material for this article can be found online at: <https://www.frontiersin.org/articles/10.3389/feart.2024.1493790/full#supplementary-material>

fluid inclusion water isotopes over the past 14,000 years. *Sci. Adv.* 5, eaav3809. doi:10.1126/sciadv.aav3809

- An, Z., Porter, S. C., Kutzbach, J. E., Xihao, W., Suming, W., Xiaodong, L., et al. (2000). Asynchronous holocene optimum of the East Asian monsoon. *Quat. Sci. Rev.* 19, 743–762. doi:10.1016/S0277-3791(99)00031-1
- Anand, P., Elderfield, H., and Conte, M. H. (2003). Calibration of Mg/Ca thermometry in planktonic foraminifera from a sediment trap time series. *Paleoceanography* 18. doi:10.1029/2002pa000846
- Anwar, T., Kravchinsky, V. A., Zhang, R., Koukhar, L. P., Yang, L., and Yue, L. (2018). Holocene climatic evolution at the Chinese Loess Plateau: testing sensitivity to the global warming-cooling events. *J. Asian Earth Sci.* 166, 223–232. doi:10.1016/j.jseas.2018.07.032
- Baker, J. L., Lachniet, M. S., Chervyatsova, O., Asmerom, Y., and Polyak, V. J. (2017). Holocene warming in western continental Eurasia driven by glacial retreat and greenhouse forcing. *Nat. Geosci.* 10, 430–435. doi:10.1038/ngeo2953
- Bard, E., Rostek, F., and Sonzogni, C. (1997). Interhemispheric synchrony of the last deglaciation inferred from alkenone palaeothermometry. *Nature* 385, 707–710. doi:10.1038/385707a0
- Berger, A. (1978). Long-term variations of caloric insolation resulting from the earth's orbital elements. *Quat. Res.* 9, 139–167. doi:10.1016/0033-5894(78)90064-9
- Böll, A., Schulz, H., Munz, P., Rixen, T., Gaye, B., and Emeis, K.-C. (2015). Contrasting sea surface temperature of summer and winter monsoon variability in the northern Arabian Sea over the last 25ka. *Paleoceanogr. Palaeoclimatol. Palaeoecol.* 426, 10–21. doi:10.1016/j.palaeo.2015.02.036
- Bosmans, J. H. C., Erb, M. P., Dolan, A. M., Drijfhout, S. S., Tuenter, E., Hilgen, F. J., et al. (2018). Response of the Asian summer monsoons to idealized precession and obliquity forcing in a set of GCMs. *Quat. Sci. Rev.* 188, 121–135. doi:10.1016/j.quascirev.2018.03.025
- Bronk, R. C. (2009). Bayesian analysis of radiocarbon dates. *Radiocarbon* 51, 337–360. doi:10.1017/S0033822200033865
- Brown, S. J., and Elderfield, H. (1996). Variations in Mg/Ca and Sr/Ca ratios of planktonic foraminifera caused by postdepositional dissolution: evidence of shallow Mg-dependent dissolution. *Paleoceanography* 11, 543–551. doi:10.1029/96pa01491
- Cai, Y., Tan, L., Cheng, H., An, Z., Edwards, R. L., Kelly, M. J., et al. (2010). The variation of summer monsoon precipitation in central China since the last deglaciation. *Earth Planet. Sci. Lett.* 291, 21–31. doi:10.1016/j.epsl.2009.12.039
- Carolin, S. A., Cobb, K. M., Adkins, J. F., Clark, B., Conroy, J. L., Lejau, S., et al. (2013). Varied response of western Pacific hydrology to climate forcings over the last glacial period. *Science* 340, 1564–1566. doi:10.1126/science.1233797
- Chawchai, S., Tan, L., Löwemark, L., Wang, H.-C., Yu, T.-L., Chung, Y.-C., et al. (2021). Hydroclimate variability of central Indo-Pacific region during the Holocene. *Quat. Sci. Rev.* 253, 106779. doi:10.1016/j.quascirev.2020.106779
- Chen, M.-T., Shiau, L.-J., Yu, P.-S., Chiu, T.-C., Chen, Y.-G., and Wei, K.-Y. (2003). 500 000-Year records of carbonate, organic carbon, and foraminiferal sea-surface temperature from the southeastern South China Sea (near Palawan Island). *Paleoceanogr. Palaeoclimatol. Palaeoecol.* 197, 113–131. doi:10.1016/S0031-0182(03)00389-4
- Chen, M.-T., Wang, C.-H., Huang, C.-Y., Wang, P., Wang, L., and Sarnthein, M. (1999). A late Quaternary planktonic foraminiferal faunal record of rapid climatic changes from the South China Sea. *Mar. Geol.* 156, 85–108. doi:10.1016/S0025-3227(98)00174-1
- Cheng, H., Edwards, R. L., Sinha, A., Spötl, C., Yi, L., Chen, S., et al. (2016). The Asian monsoon over the past 640,000 years and ice age terminations. *Nature* 534, 640–646. doi:10.1038/nature18591
- Cheng, H., Zhang, H., Cai, Y., Shi, Z., Yi, L., Deng, C., et al. (2021). Orbital-scale Asian summer monsoon variations: paradox and exploration. *Sci. China Earth Sci.* 64, 529–544. doi:10.1007/s11430-020-9720-y
- Cheng, H., Zhang, H., Zhao, J., Li, H., Ning, Y., and Kathayat, G. (2019). Chinese stalagmite paleoclimate researches: a review and perspective. *Sci. China Earth Sci.* 62, 1489–1513. doi:10.1007/s11430-019-9478-3
- Chiang, J. C. H., and Friedman, A. R. (2012). Extratropical cooling, interhemispheric thermal gradients, and tropical climate change. *Annu. Rev. Earth Planet. Sci.* 40, 383–412. doi:10.1146/annurev-earth-042711-105545
- Chiang, J. C. H., Fung, I. Y., Wu, C.-H., Cai, Y., Edman, J. P., Liu, Y., et al. (2015). Role of seasonal transitions and westerly jets in East Asian paleoclimate. *Quat. Sci. Rev.* 108, 111–129. doi:10.1016/j.quascirev.2014.11.009
- Clemens, S. C., Prell, W. L., and Sun, Y. (2010). Orbital-scale timing and mechanisms driving Late Pleistocene Indo-Asian summer monsoons: reinterpreting cave speleothem  $\delta^{18}O$ . *Paleoceanography* 25. doi:10.1029/2010pa001926
- Clemens, S. C., Prell, W. L., Sun, Y., Liu, Z., and Chen, G. (2008). Southern hemisphere forcing of Pliocene  $\delta^{18}O$  and the evolution of Indo-Asian monsoons. *Paleoceanography* 23. doi:10.1029/2008pa001638
- Dang, H., Jian, Z., Wang, Y., Mohtadi, M., Rosenthal, Y., Ye, L., et al. (2020). Pacific warm pool subsurface heat sequestration modulated Walker circulation and ENSO activity during the Holocene. *Sci. Adv.* 6, eabc0402. doi:10.1126/sciadv.abc0402
- Dekens, P. S., Lea, D. W., Pak, D. K., and Spero, H. J. (2002). Core top calibration of Mg/Ca in tropical foraminifera: refining paleotemperature estimation. *Geochem. Geophys. Geosystems* 3, 1–29. doi:10.1029/2001gc000200
- Dong, J., Li, A., Lu, Z., Liu, X., Wan, S., Yan, H., et al. (2021). Millennial-scale interaction between the East Asian winter monsoon and El Niño-related tropical Pacific precipitation in the Holocene. *Paleoceanogr. Palaeoclimatol. Palaeoecol.* 573, 110442. doi:10.1016/j.palaeo.2021.110442
- Dong, J., Shen, C.-C., Kong, X., Wang, H.-C., and Jiang, X. (2015). Reconciliation of hydroclimate sequences from the Chinese loess plateau and low-latitude East Asian summer monsoon regions over the past 14,500 years. *Paleoceanogr. Palaeoclimatol. Palaeoecol.* 435, 127–135. doi:10.1016/j.palaeo.2015.06.013
- Dong, J., Shen, C.-C., Kong, X., Wu, C.-C., Hu, H.-M., Ren, H., et al. (2018). Rapid retreat of the East Asian summer monsoon in the middle Holocene and a millennial weak monsoon interval at 9 ka in northern China. *J. Asian Earth Sci.* 151, 31–39. doi:10.1016/j.jseas.2017.10.016
- Dong, J., Wang, Y., Cheng, H., Hardt, B., Edwards, R. L., Kong, X., et al. (2010). A high-resolution stalagmite record of the Holocene East Asian monsoon from Mt Shennongjia, central China. *Holocene* 20, 257–264. doi:10.1177/0959683609350393
- Du, X., Hendy, L., Hinnov, L., Brown, E., Zhu, J., and Poulsen, C. J. (2021). High-resolution interannual precipitation reconstruction of Southern California: implications for Holocene ENSO evolution. *Earth Planet. Sci. Lett.* 554, 116670. doi:10.1016/j.epsl.2020.116670
- Dutt, S., Gupta, A. K., Clemens, S. C., Cheng, H., Singh, R. K., Kathayat, G., et al. (2015). Abrupt changes in Indian summer monsoon strength during 33,800 to 5500 years B.P. *B.P. Geophys. Res. Lett.* 42, 5526–5532. doi:10.1002/2015gl064015
- Dykoski, C. A., Edwards, R. L., Cheng, H., Yuan, D., Cai, Y., Zhang, M., et al. (2005). A high-resolution, absolute-dated Holocene and deglacial Asian monsoon record from Dongge Cave, China. *Earth Planet. Sci. Lett.* 233, 71–86. doi:10.1016/j.epsl.2005.01.036
- Eggins, S., Deckker, P. D., and Marshall, J. (2003). Mg/Ca variation in planktonic foraminifera tests: implications for reconstructing palaeo-seawater temperature and habitat migration. *Earth Planet. Sci. Lett.* 212, 291–306. doi:10.1016/S0012-821X(03)00283-8
- Fan, W., Jian, Z., Bassinot, F., and Chu, Z. (2013). Holocene centennial-scale changes of the Indonesian and south China sea throughflows: evidences from the makassar strait. *Glob. Planet. Change* 111, 111–117. doi:10.1016/j.gloplacha.2013.08.017
- Fehrenbacher, J. S., Spero, H. J., Russell, A. D., Vetter, L., and Eggins, S. (2015). Optimizing LA-ICP-MS analytical procedures for elemental depth profiling of foraminifera shells. *Chem. Geol.* 407–408, 2–9. doi:10.1016/j.chemgeo.2015.04.007
- Fleitmann, D., Burns, S. J., Mangini, A., Mudelsee, M., Kramers, J., Villa, I., et al. (2007). Holocene ITCZ and Indian monsoon dynamics recorded in stalagmites from Oman and Yemen (Socotra). *Quat. Sci. Rev.* 26, 170–188. doi:10.1016/j.quascirev.2006.04.012
- Fleitmann, D., Burns, S. J., Mudelsee, M., Neff, U., Kramers, J., Mangini, A., et al. (2003). Holocene forcing of the Indian monsoon recorded in a stalagmite from southern Oman. *Science* 300, 1737–1739. doi:10.1126/science.1083130
- Ford, H. L., Ravelo, A. C., and Polissar, P. J. (2015). Reduced El Niño-southern oscillation during the last glacial maximum. *Science* 347, 255–258. doi:10.1126/science.1258437
- Gebregiorgis, D., Hathorne, E. C., Giosan, L., Clemens, S., Nürnberg, D., and Frank, M. (2018). Southern Hemisphere forcing of South Asian monsoon precipitation over the past ~1 million years. *Nat. Commun.* 9, 4702. doi:10.1038/s41467-018-07076-2
- Gebregiorgis, D., Hathorne, E. C., Sijinkumar, A. V., Nath, B. N., Nürnberg, D., and Frank, M. (2016). South Asian summer monsoon variability during the last ~54 kys inferred from surface water salinity and river runoff proxies. *Quat. Sci. Rev.* 138, 6–15. doi:10.1016/j.quascirev.2016.02.012
- Govil, P., and Divakar, N. P. (2011). Variations of Indian monsoon precipitation during the last 32kyr reflected in the surface hydrography of the Western Bay of Bengal. *Quat. Sci. Rev.* 30, 3871–3879. doi:10.1016/j.quascirev.2011.10.004
- Groeneveld, J., Ho, S. L., Mackensen, A., Mohtadi, M., and Laepple, T. (2019). Deciphering the variability in Mg/Ca and stable oxygen isotopes of individual foraminifera. *Paleoceanogr. Palaeoclimatol.* 34, 755–773. doi:10.1029/2018pa003533
- Groeneveld, J., Nürnberg, D., Tiedemann, R., Reichert, G.-J., Steph, S., Reuning, L., et al. (2008). Foraminiferal Mg/Ca increase in the Caribbean during the Pleocene: western atlantic warm pool formation, salinity influence, or diagenetic overprint? *Geochem. Geophys. Geosystems* 9, 1–21. doi:10.1029/2006gc001564
- Haug, G. H., Hughen, K. A., Sigman, D. M., Peterson, L. C., and Röhl, U. (2001). Southward migration of the intertropical convergence zone through the holocene. *Science* 293, 1304–1308. doi:10.1126/science.1059725
- He, J., Zhao, M., Li, L., Wang, P., and Ge, H. (2008). Sea surface temperature and terrestrial biomarker records of the last 260 ka of core MD05-2904 from the northern South China Sea. *Chinese Science Bulletin* 53, 2376–2384. doi:10.1007/s11434-008-0289-2
- Heaton, T. J., Köhler, P., Butzin, M., Bard, E., Reimer, R. W., Austin, W. E. N., et al. (2020). Marine20—the marine radiocarbon age calibration curve (0–55,000 cal BP). *Radiocarbon* 62, 779–820. doi:10.1017/rdc.2020.68
- Hori, M. E., and Ueda, H. (2006). Impact of global warming on the East Asian winter monsoon as revealed by nine coupled atmosphere-ocean GCMs. *Geophys. Res. Lett.* 33. doi:10.1029/2005gl024961

- Hu, C., Henderson, G. M., Huang, J., Xie, S., Sun, Y., and Johnson, K. R. (2008). Quantification of Holocene Asian monsoon rainfall from spatially separated cave records. *Earth Planet. Sci. Lett.* 266, 221–232. doi:10.1016/j.epsl.2007.10.015
- Hu, Z.-Z., Bengtsson, L., and Arpe, K. (2000). Impact of global warming on the Asian winter monsoon in a coupled GCM. *J. Geophys. Res. Atmos.* 105, 4607–4624. doi:10.1029/1999jd901031
- Huang, C.-Y., Wu, S.-F., Zhao, M., Chen, M.-T., Wang, C.-H., Tu, X., et al. (1997). Surface ocean and monsoon climate variability in the South China Sea since the last glaciation. *Mar. Micropaleontol.* 32, 71–94. doi:10.1016/s0377-8398(97)00014-5
- Huang, E., Tian, J., and Steinke, S. (2011). Millennial-scale dynamics of the winter cold tongue in the southern South China Sea over the past 26ka and the East Asian winter monsoon. *Quat. Res.* 75, 196–204. doi:10.1016/j.yqres.2010.08.014
- Huang, E., Wang, P., Wang, Y., Yan, M., Tian, J., Li, S., et al. (2020). Dole effect as a measurement of the low-latitude hydrological cycle over the past 800 ka. *Sci. Adv.* 6, eaba4823. doi:10.1126/sciadv.aba4823
- Huang, J., Li, A., and Wan, S. (2011). Sensitive grain-size records of Holocene East Asian summer monsoon in sediments of northern South China Sea slope. *Quat. Res.* 75, 734–744. doi:10.1016/j.yqres.2011.03.002
- Huang, J., Wan, S., Xiong, Z., Zhao, D., Liu, X., Li, A., et al. (2016). Geochemical records of Taiwan-sourced sediments in the South China Sea linked to Holocene climate changes. *Palaeogeogr. Palaeoclimatol. Palaeoecol.* 441, 871–881. doi:10.1016/j.palaeo.2015.10.036
- Huang, R., C. C., Chen, G., Chen, M.-T., Lee, K., M, Y., et al. (2002). Planktic foraminifer faunal sea surface temperature records of the past two glacial terminations in the South China Sea near Wan-An Shallow (IMAGES Core MD972151). *Austrian J. Earth Sci.* 2, 1–14. doi:10.1594/PANGAEA.65424
- Huang, R. H., Chen, W., Yang, B. L., and Zhang, R. H. (2004). Recent advances in studies of the interaction between the East Asian winter and summer monsoons and ENSO cycle. *Adv. Atmos. Sci.* 21, 407–424. doi:10.1007/bf02915568
- Huang, Y., Jiang, H., Sarnthein, M., Knudsen, K. L., and Li, D. (2009). Diatom response to changes in palaeoenvironments of the northern South China Sea during the last 15000 years. *Mar. Micropaleontol.* 72, 99–109. doi:10.1016/j.marmicro.2009.04.003
- Imbrie, J., Boyle, E. A., Clemens, S. C., Duffy, A., Howard, W. R., Kukla, G., et al. (1992). On the structure and origin of major glaciation cycles 1. Linear responses to milankovitch forcing. *Paleoceanography* 7, 701–738. doi:10.1029/92pa02253
- Jia, G., Bai, Y., Yang, X., Xie, L., Wei, G., Ouyang, T., et al. (2015). Biogeochemical evidence of Holocene East Asian summer and winter monsoon variability from a tropical maar lake in southern China. *Quat. Sci. Rev.* 111, 51–61. doi:10.1016/j.quascirev.2015.01.002
- Jia, Y.-n., Zhang, Y., Wang, N., Chang Huang, C., Qiu, H., Wang, H., et al. (2021). Chronostratigraphic framework and paleoenvironmental interpretation of the Holocene loess-paleosol sequence in the Luoyang Basin, Central China. *Aeolian Res.* 48, 100657. doi:10.1016/j.aeolia.2020.100657
- Jochum, K. P., Jentzen, A., Schiebel, R., Stoll, B., Weis, U., Leitner, J., et al. (2019). High-resolution Mg/Ca measurements of foraminifer shells using femtosecond LA-ICPMS for paleoclimate proxy development. *Geochem. Geophys. Geosyst.* 20, 2053–2063. doi:10.1029/2018gc008091
- Kaboth-Bahr, S., Bahr, A., Yamoah, K. A., Chuang, C.-K., Li, H.-C., Su, C.-C., et al. (2021a). Rapid humidity changes across the Northern South China Sea during the last ~40 kyr. *Mar. Geol.* 440, 106579. doi:10.1016/j.margeo.2021.106579
- Kaboth-Bahr, S., Bahr, A., Zeeden, C., Yamoah, K. A., Lone, M. A., Chuang, C.-K., et al. (2021b). A tale of shifting relations: East Asian summer and winter monsoon variability during the Holocene. *Sci. Rep.* 11, 6938. doi:10.1038/s41598-021-85444-7
- Kienast, M., Steinke, S., Statterger, K., and Calvert, S. E. (2001). Synchronous tropical south China sea SST change and Greenland warming during deglaciation. *Science* 291, 2132–2134. doi:10.1126/science.1057131
- Kong, D., Zong, Y., Jia, G., Wei, G., Chen, M.-T., and Liu, Z. (2014). The development of late Holocene coastal cooling in the northern South China Sea. *Quat. Int.* 349, 300–307. doi:10.1016/j.quaint.2013.08.055
- Kong, W., Swenson, L. M., and Chiang, J. C. H. (2017). Seasonal transitions and the westerly jet in the holocene East Asian summer monsoon. *J. Clim.* 30, 3343–3365. doi:10.1175/jcli-d-16-0087.1
- Krause, C. E., Gagan, M. K., Dunbar, G. B., Hantoro, W. S., Hellstrom, J. C., Cheng, H., et al. (2019). Spatio-temporal evolution of Australasian monsoon hydroclimate over the last 40,000 years. *Earth Planet. Sci. Lett.* 513, 103–112. doi:10.1016/j.epsl.2019.01.045
- Laskar, J., Robutel, P., Joutel, F., Gastineau, M., Correia, A. C. M., and Levrard, B. (2004). A long-term numerical solution for the insolation quantities of the Earth. *A&A* 428, 261–285. doi:10.1051/0004-6361/20041335
- Lauterbach, S., Andersen, N., Wang, Y. V., Blanz, T., Larsen, T., and Schneider, R. R. (2020). An ~130 kyr record of surface water temperature and  $\delta^{18}O$  from the northern bay of bengal: investigating the linkage between heinrich events and weak monsoon intervals in Asia. *Paleoceanogr. Paleoclimatology* 35, e2019PA003646. doi:10.1029/2019pa003646
- Leduc, G., Schneider, R., Kim, J. H., and Lohmann, G. (2010). Holocene and Eemian sea surface temperature trends as revealed by alkenone and Mg/Ca paleothermometry. *Quat. Sci. Rev.* 29, 989–1004. doi:10.1016/j.quascirev.2010.01.004
- Lee, J.-E., Baylor, F.-K., Horvat, C., and Ming, Y. (2019). The response of East Asian monsoon to the precessional cycle: a new study using the geophysical fluid dynamics laboratory model. *Geophys. Res. Lett.* 46, 11388–11396. doi:10.1029/2019gl026661
- Levi, C., Labeyrie, L., Bassinot, F., Guichard, F., Cortijo, E., Waelbroeck, C., et al. (2007). Low-latitude hydrological cycle and rapid climate changes during the last deglaciation. *Geochem. Geophys. Geosystems* 8. doi:10.1029/2006gc001514
- Li, M., Ouyang, T., Tian, C., Zhu, Z., Peng, S., Tang, Z., et al. (2019). Sedimentary responses to the East Asian monsoon and sea level variations recorded in the northern South China Sea over the past 36 kyr. *J. Asian Earth Sci.* 171, 213–224. doi:10.1016/j.jseaes.2018.01.001
- Lin, Y.-S., Wei, K.-Y., Lin, I.-T., Yu, P.-S., Chiang, H.-W., Chen, C.-Y., et al. (2006). The holocene pulleniatina minimum event revisited: geochemical and faunal evidence from the okinawa trough and upper reaches of the kuroshio current. *Mar. Micropaleontol.* 59, 153–170. doi:10.1016/j.marmicro.2006.02.003
- Linsley, B. K., Rosenthal, Y., and Oppo, D. W. (2010). Holocene evolution of the Indonesian throughflow and the western Pacific warm pool. *Nat. Geosci.* 3, 578–583. doi:10.1038/ngeo920
- Liu, Y., Zhang, M., Liu, Z., Xia, Y., Huang, Y., Peng, Y., et al. (2018). A possible role of dust in resolving the holocene temperature conundrum. *Sci. Rep.* 8, 4434. doi:10.1038/s41598-018-22841-5
- Liu, Z., Wen, X., Brady, E. C., Otto-Bliesner, B., Yu, G., Lu, H., et al. (2014a). Chinese cave records and the East Asia summer monsoon. *Quat. Sci. Rev.* 83, 115–128. doi:10.1016/j.quascirev.2013.10.021
- Liu, Z., Zhu, J., Rosenthal, Y., Zhang, X., Otto-Bliesner, B. L., Timmermann, A., et al. (2014b). The Holocene temperature conundrum. *Proc. Natl. Acad. Sci.* 111, E3501–E3505. doi:10.1073/pnas.1407229111
- Lo, L., Lai, Y.-H., Wei, K.-Y., Lin, Y.-S., Mii, H.-S., and Shen, C.-C. (2013). Persistent sea surface temperature and declined sea surface salinity in the northwestern tropical Pacific over the past 7500years. *J. Asian Earth Sci.* 66, 234–239. doi:10.1016/j.jseaes.2013.01.014
- Lüthi, D., Le Floch, M., Bereiter, B., Blunier, T., Barnola, J.-M., Siegenthaler, U., et al. (2008). High-resolution carbon dioxide concentration record 650,000–800,000 years before present. *Nature* 453, 379–382. doi:10.1038/nature06949
- Ma, T., Chen, W., Feng, J., and Wu, R. (2018). Modulation effects of the East Asian winter monsoon on El Niño-related rainfall anomalies in southeastern China. *Sci. Rep.* 8, 14107. doi:10.1038/s41598-018-32492-1
- Marchitto, T. M. (2006). Precise multielemental ratios in small foraminiferal samples determined by sector field ICP-MS. *Geochem. Geophys. Geosystems* 7, 13. doi:10.1029/2005gc001018
- Marcott, S. A., Shakun, J. D., Clark, P. U., and Mix, A. C. (2013). A reconstruction of regional and global temperature for the past 11,300 years. *Science* 339, 1198–1201. doi:10.1126/science.1228026
- Marsicek, J., Shuman, B. N., Bartlein, P. J., Shafer, S. L., and Brewer, S. (2018). Reconciling divergent trends and millennial variations in Holocene temperatures. *Nature* 554, 92–96. doi:10.1038/nature25464
- Mohtadi, M., Prange, M., Oppo, D. W., De Pol-Holz, R., Merkel, U., Zhang, X., et al. (2014). North Atlantic forcing of tropical Indian Ocean climate. *Nature* 509, 76–80. doi:10.1038/nature13196
- Mohtadi, M., Steinke, S., Lückge, A., Groeneveld, J., and Hathorne, E. C. (2010). Glacial to Holocene surface hydrography of the tropical eastern Indian Ocean. *Earth Planet. Sci. Lett.* 292, 89–97. doi:10.1016/j.epsl.2010.01.024
- Nürnberg, D., Bijma, J., and Hemleben, C. (1996). Assessing the reliability of magnesium in foraminiferal calcite as a proxy for water mass temperatures. *Geochim. Cosmochim. Acta.* 60, 803–814. doi:10.1016/0016-7037(95)00446-7
- Oppo, D. W., and Sun, Y. (2005). Amplitude and timing of sea-surface temperature change in the northern South China Sea: dynamic link to the East Asian monsoon. *Geology* 33, 785–788. doi:10.1130/g21867.1
- Ramsey, C. B., and Lee, S. (2013). Recent and planned developments of the program OxCal. *Radiocarbon* 55, 720–730. doi:10.1017/s0033822200057878
- Rao, Z., Jia, G., Li, Y., Chen, J., Xu, Q., and Chen, F. (2016). Asynchronous evolution of the isotopic composition and amount of precipitation in north China during the Holocene revealed by a record of compound-specific carbon and hydrogen isotopes of long-chain n-alkanes from an alpine lake. *Earth Planet. Sci. Lett.* 446, 68–76. doi:10.1016/j.epsl.2016.04.027
- Rashid, H., Flower, B. P., Poore, R. Z., and Quinn, T. M. (2007). A ~25ka Indian Ocean monsoon variability record from the Andaman Sea. *Quat. Sci. Rev.* 26, 2586–2597. doi:10.1016/j.quascirev.2007.07.002
- Raza, T., Ahmad, S. M., Steinke, S., Raza, W., Lone, M. A., Beja, S. K., et al. (2017). Glacial to Holocene changes in sea surface temperature and seawater  $\delta^{18}O$  in the northern Indian Ocean. *Palaeogeogr. Palaeoclimatol. Palaeoecol.* 485, 697–705. doi:10.1016/j.palaeo.2017.07.026

- Rongstad, B. L., Marchitto, T. M., and Herguera, J. C. (2017). Understanding the effects of dissolution on the Mg/Ca paleothermometer in planktic foraminifera: evidence from a novel individual foraminifera method. *Paleoceanography* 32, 1386–1402. doi:10.1002/2017pa003179
- Rosenthal, Y., Boyle, E. A., and Slowey, N. (1997). Temperature control on the incorporation of magnesium, strontium, fluorine, and cadmium into benthic foraminiferal shells from Little Bahama Bank: prospects for thermocline paleoceanography. *Geochim. Cosmochim. Acta.* 61, 3633–3643. doi:10.1016/s0016-7037(97)00181-6
- Rostek, F., Bard, E., Beaufort, L., Sonzogni, C., and Ganssen, G. (1997). Sea surface temperature and productivity records for the past 240 kyr in the Arabian Sea. *Deep Sea Res. Part II Top. Stud. Oceanogr.* 44, 1461–1480. doi:10.1016/s0967-0645(97)00008-8
- Ruan, J., Zhang, H., Cai, Z., Yang, X., and Yin, J. (2019). Regional controls on daily to interannual variations of precipitation isotope ratios in Southeast China: implications for paleomonsoon reconstruction. *Earth Planet. Sci. Lett.* 527, 115794. doi:10.1016/j.epsl.2019.115794
- Rustic, G. T., Polissar, P. J., Ravelo, A. C., and DeMenocal, P. (2021). Relationship between individual chamber and whole shell Mg/Ca ratios in *Trilobatus sacculifer* and implications for individual foraminifera palaeoceanographic reconstructions. *Sci. Rep.* 11, 463. doi:10.1038/s41598-020-80673-8
- Rustic, G. T., Polissar, P. J., Ravelo, A. C., and White, S. M. (2020). Modulation of late Pleistocene ENSO strength by the tropical Pacific thermocline. *Nat. Commun.* 11, 5377. doi:10.1038/s41467-020-19161-6
- Sadekov, A., Eggins, S. M., De Deckker, P., Ninnemann, U., Kuhnt, W., and Bassinot, F. (2009). Surface and subsurface seawater temperature reconstruction using Mg/Ca microanalysis of planktonic foraminifera *Globigerinoides ruber*, *Globigerinoides sacculifer*, and *Pulleniatina obliquiloculata*. *Paleoceanography* 24. doi:10.1029/2008pa001664
- Sadekov, A. Y., Eggins, S. M., Klinkhammer, G. P., and Rosenthal, Y. (2010). Effects of seafloor and laboratory dissolution on the Mg/Ca composition of *Globigerinoides sacculifer* and *Orbulina universa* tests — a laser ablation ICPMS microanalysis perspective. *Earth Planet. Sci. Lett.* 292, 312–324. doi:10.1016/j.epsl.2010.01.039
- Saraswat, R., Lea, D. W., Nigam, R., Mackensen, A., and Naik, D. K. (2013). Deglaciation in the tropical Indian Ocean driven by interplay between the regional monsoon and global teleconnections. *Earth Planet. Sci. Lett.* 375, 166–175. doi:10.1016/j.epsl.2013.05.022
- Selvaraj, K., Chen, C. T. A., and Lou, J.-Y. (2007). Holocene East Asian monsoon variability: links to solar and tropical Pacific forcing. *Geophys. Res. Lett.* 34. doi:10.1029/2006gl028155
- Setiawan, R., Southon, J., Groeneweld, J., Steinke, S., and Hebbeln, D. (2015). The consequences of opening the Sunda Strait on the hydrography of the eastern tropical Indian Ocean. *Paleoceanography* 30, 1358–1372. doi:10.1002/2015pa002802
- Steinke, S., Chiu, H.-Y., Yu, P.-S., Shen, C.-C., Erlenkeuser, H., Löwemark, L., et al. (2006). On the influence of sea level and monsoon climate on the southern South China Sea freshwater budget over the last 22,000 years. *Quat. Sci. Rev.* 25, 1475–1488. doi:10.1016/j.quascirev.2005.12.008
- Steinke, S., Kienast, M., Groeneweld, J., Lin, L.-C., Chen, M.-T., and Rendle-Bühning, R. (2008). Proxy dependence of the temporal pattern of deglacial warming in the tropical South China Sea: toward resolving seasonality. *Quat. Sci. Rev.* 27, 688–700. doi:10.1016/j.quascirev.2007.12.003
- Stott, L., Cannariato, K., Thunell, R., Haug, G. H., Koutavas, A., and Lund, S. (2004). Decline of surface temperature and salinity in the western tropical Pacific Ocean in the Holocene epoch. *Nature* 431, 56–59. doi:10.1038/nature02903
- Stott, L., Timmermann, A., and Thunell, R. (2007). Southern hemisphere and deep-sea warming led deglacial atmospheric CO<sub>2</sub> rise and tropical warming. *Science* 318, 435–438. doi:10.1126/science.1143791
- Tian, Z., Li, T., and Jiang, D. (2018). Strengthening and westward shift of the tropical Pacific Walker circulation during the mid-holocene: PMIP simulation results. *J. Clim.* 31, 2283–2298. doi:10.1175/jcli-d-16-0744.1
- Tierney, J. E., Malevich, S. B., Gray, W., Vetter, L., and Thirumalai, K. (2019). Bayesian calibration of the Mg/Ca paleothermometer in planktic foraminifera. *Paleoceanogr. Paleoclimatol.* 34, 2005–2030. doi:10.1029/2019pa003744
- Tiwari, M., Nagoji, S. S., and Ganeshram, R. S. (2015). Multi-centennial scale SST and Indian summer monsoon precipitation variability since the mid-Holocene and its nonlinear response to solar activity. *Holocene* 25, 1415–1424. doi:10.1177/0959683615585840
- Vetter, L., Spero, H. J., Russell, A. D., and Fehrenbacher, J. S. (2013). LA-ICP-MS depth profiling perspective on cleaning protocols for elemental analyses in planktic foraminifera. *Geochem. Geophys. Geosystems* 14, 2916–2931. doi:10.1002/ggge.20163
- Wang, H., Chen, J., Zhang, X., and Chen, F. (2014). Palaeosol development in the Chinese Loess Plateau as an indicator of the strength of the East Asian summer monsoon: evidence for a mid-Holocene maximum. *Quat. Int.* 334–335, 155–164. doi:10.1016/j.quaint.2014.03.013
- Wang, L., Lu, H., Liu, J., Gu, Z., Mingram, J., Chu, G., et al. (2008). Diatom-based inference of variations in the strength of Asian winter monsoon winds between 17,500 and 6000 calendar years B.P. *J. Geophys. Res. Atmos.* 113. doi:10.1029/2008jd010145
- Wang, L., Sarnthein, M., Erlenkeuser, H., Grimalt, J., Grootes, P., Heilig, S., et al. (1999). East Asian monsoon climate during the late pleistocene: high-resolution sediment records from the South China sea. *Mar. Geol.* 156, 245–284. doi:10.1016/s0025-3227(98)00182-0
- Wang, N., Jiang, D., and Lang, X. (2020). Mechanisms for spatially inhomogeneous changes in East Asian summer monsoon precipitation during the mid-holocene. *J. Clim.* 33, 2945–2965. doi:10.1175/jcli-d-19-0565.1
- Wang, P. X., Wang, B., Cheng, H., Fasullo, J., Guo, Z., Kiefer, T., et al. (2017). The global monsoon across time scales: mechanisms and outstanding issues. *Earth-Science Rev.* 174, 84–121. doi:10.1016/j.earscirev.2017.07.006
- Wang, Y., Jian, Z. M., Zhao, P., Xiao, D., and Chen, J. M. (2016). Relative roles of land-and ocean-atmosphere interactions in Asian-Pacific thermal contrast variability at the precessional band. *Sci. Rep.* 6, 28349. doi:10.1038/srep28349
- Wang, Y. J., Cheng, H., Edwards, R. L., An, Z. S., Wu, J. Y., Shen, C.-C., et al. (2001). A high-resolution absolute-dated late pleistocene monsoon record from hulu cave, China. *Science* 294, 2345–2348. doi:10.1126/science.1064618
- Wei, G., Deng, W., Liu, Y., and Li, X. (2007). High-resolution sea surface temperature records derived from foraminiferal Mg/Ca ratios during the last 260 ka in the northern South China Sea. *Paleogeogr. Paleoclimatol. Paleoecol.* 250, 126–138. doi:10.1016/j.palaeo.2007.03.005
- Wen, X., Liu, Z., Wang, S., Cheng, J., and Zhu, J. (2016). Correlation and anti-correlation of the East Asian summer and winter monsoons during the last 21,000 years. *Nat. Commun.* 7, 11999. doi:10.1038/ncomms11999
- White, S. M., Ravelo, A. C., and Polissar, P. J. (2018). Dampened El Niño in the early and mid-holocene due to insolation-forced warming/deepening of the thermocline. *Geophys. Res. Lett.* 45, 316–326. doi:10.1002/2017gl075333
- Wu, X., Zhang, Z., Xu, X., and Shen, J. (2012). Asian summer monsoonal variations during the Holocene revealed by Huguangyan maar lake sediment record. *Paleogeogr. Paleoclimatol. Paleoecol.* 323–325, 13–21. doi:10.1016/j.palaeo.2012.01.020
- Wu, Y., Li, T.-Y., Yu, T.-L., Shen, C.-C., Chen, C.-J., Zhang, J., et al. (2020). Variation of the Asian summer monsoon since the last glacial-interglacial recorded in a stalagmite from southwest China. *Quat. Sci. Rev.* 234, 106261. doi:10.1016/j.quascirev.2020.106261
- Wurtzel, J. B., Abram, N. J., Lewis, S. C., Bajo, P., Hellstrom, J. C., Troitzsch, U., et al. (2018). Tropical Indo-Pacific hydroclimate response to North Atlantic forcing during the last deglaciation as recorded by a speleothem from Sumatra, Indonesia. *Earth Planet. Sci. Lett.* 492, 264–278. doi:10.1016/j.epsl.2018.04.001
- Yang, J., Zhao, Y., Wei, H., Liu, S., Zhang, G., Long, H., et al. (2023). Holocene sea surface temperature and salinity variations in the central South China Sea. *Mar. Micropaleontol.* 181, 102229. doi:10.1016/j.marmicro.2023.102229
- Yang, X., Yang, H., Wang, B., Huang, L.-J., Shen, C.-C., Edwards, R. L., et al. (2019a). Early-Holocene monsoon instability and climatic optimum recorded by Chinese stalagmites. *Holocene* 29, 1059–1067. doi:10.1177/0959683619831433
- Yang, Y., Xiang, R., Liu, J., and Tang, L. (2019b). Inconsistent sea surface temperature and salinity changing trend in the northern South China Sea since 7.0 ka BP. *J. Asian Earth Sci.* 171, 178–186. doi:10.1016/j.jseas.2018.05.033
- Yim, S.-Y., Wang, B., and Kwon, M. (2014). Interdecadal change of the controlling mechanisms for East Asian early summer rainfall variation around the mid-1990s. *Clim. Dyn.* 42, 1325–1333. doi:10.1007/s00382-013-1760-6
- Yin, J., Yang, X., Zhou, Q., Li, G., Gao, H., and Liu, J. (2021). Sea surface temperature and salinity variations from the end of last glacial maximum (LGM) to the holocene in the northern south China Sea. *Paleogeogr. Paleoclimatol. Paleoecol.* 562, 110102. doi:10.1016/j.palaeo.2020.110102
- Yokoyama, Y., Suzuki, A., Siringan, F., Maeda, Y., Abe-Ouchi, A., Ohgaito, R., et al. (2011). Mid-Holocene palaeoceanography of the northern South China Sea using coupled fossil-modern coral and atmosphere-ocean GCM model. *Geophys. Res. Lett.* 38. doi:10.1029/2010gl044231
- Zhang, H., Zhang, X., Cai, Y., Sinha, A., Spötl, C., Baker, J., et al. (2021). A data-model comparison pinpoints Holocene spatiotemporal pattern of East Asian summer monsoon. *Quat. Sci. Rev.* 261, 106911. doi:10.1016/j.quascirev.2021.106911
- Zhang, Y., Renssen, H., Seppä, H., and Valdes, P. J. (2018). Holocene temperature trends in the extratropical Northern Hemisphere based on inter-model comparisons. *J. Quat. Sci.* 33, 464–476. doi:10.1002/jqs.3027
- Zhao, M., Huang, C.-Y., Wang, C.-C., and Wei, G. (2006). A millennial-scale U37K' sea-surface temperature record from the South China Sea (8°N) over the last 150 kyr: monsoon and sea-level influence. *Paleogeogr. Paleoclimatol. Paleoecol.* 236, 39–55. doi:10.1016/j.palaeo.2005.11.033
- Zhong, W., Cao, J., Xue, J., Ouyang, J., Tang, X., Yin, H., et al. (2014). Late Holocene monsoon climate as evidenced by proxy records from a lacustrine sediment sequence in western Guangdong, South China. *J. Asian Earth Sci.* 80, 56–62. doi:10.1016/j.jseas.2013.10.030
- Zhou, X., Sun, L., Zhan, T., Huang, W., Zhou, X., Hao, Q., et al. (2016). Time-transgressive onset of the holocene optimum in the East Asian monsoon region. *Earth Planet. Sci. Lett.* 456, 39–46. doi:10.1016/j.epsl.2016.09.052